



Heterotypic Scaffold Design Orchestrates Primary Cell Organization and Phenotypes in Cocultured Small Diameter Vascular Grafts

Tomasz Jungst, Iris Pennings, Michael Schmitz, Antoine J. W. P. Rosenberg, Jürgen Groll,* and Debby Gawlitta*

To facilitate true regeneration, a vascular graft should direct the evolution of a neovessel to obtain the function of a native vessel. For this, scaffolds have to permit the formation of an intraluminal endothelial cell monolayer, mimicking the tunica intima. In addition, when attempting to mimic a tunica media-like outer layer, the stacking and orientation of vascular smooth muscle cells (vSMCs) should be recapitulated. An integral scaffold design that facilitates this has so far remained a challenge. A hybrid fabrication approach is introduced by combining solution electrospinning and melt electrowriting. This allows a tissue-structure mimetic, hierarchically bilayered tubular scaffold, comprising an inner layer of randomly oriented dense fiber mesh and an outer layer of microfibers with controlled orientation. The scaffold supports the organization of a continuous luminal endothelial monolayer and oriented layers of vSM-like cells in the media, thus facilitating control over specific and tissue-mimetic cellular differentiation and support of the phenotypic morphology in the respective layers. Neither soluble factors nor a surface bioactivation of the scaffold is needed with this approach, demonstrating that heterotypic scaffold design can direct physiological tissue-like cell organization and differentiation.

1. Introduction

Vascular grafts with improved long-term efficacy are a great clinical demand. Especially the replacement of small diameter blood vessels (<6 mm) remains a major challenge, due to problems associated with occlusion of the grafts, intimal hyperplasia, or thrombosis.^[1] The current clinical gold standard is to use autologous vessels, which is restricted by limited availability. Due to this and other limitations, biofabrication is a promising alternative approach for creating vascular grafts.

Natural blood vessels are, inter alia, comprised of a luminal layer (tunica intima) containing a single antithrombogenic monolayer of endothelial cells (ECs) attached to their basement membrane,^[1] and a secondary contractile medial layer containing near-circumferentially oriented vascular smooth muscle cells (vSMCs) which are embedded in an independent basement membrane matrix (tunica media).^[2] Efforts for tissue engineering of vascular grafts are


mostly focused on recreating these two layers and result in bilayered scaffolds.

Approaches for creating vascular grafts can rely on scaffolds, on soft hydrogels, or composites thereof^[3] and numerous studies have demonstrated promising results in the field of vascular tissue regeneration. Examples for studies that have shown promising in vivo performance include completely biological hydrogels in the form of human cell-based sheets^[4] and on biopolymer-based attempts in the form of hydrogels.^[5] Despite the promising performance, those approaches rely on time-consuming and often manual fabrication. Here, scaffold-based approaches are of advantage, which also offer the possibility to improve cell-material interactions and true hierarchical biomimicry of the native morphology in the constructs.

Among the applied fabrication methods, electrospinning of polymer solutions (solution electrospinning, SES), a process that predominantly yields nonwoven mats of fibers with diameters in a nanometer to micrometer range, has received considerable attention.^[1a,6] The morphology of SES scaffolds can be adjusted as the fiber diameter influences the pore size of

Dr. T. Jungst, Dr. M. Schmitz, Prof. J. Groll
Department for Functional Materials in Medicine and Dentistry
and Bavarian Polymer Institute
University of Würzburg
Pleicherwall 2, 97070 Würzburg, Germany
E-mail: juergen.groll@fmz.uni-wuerzburg.de

I. Pennings, Prof. A. J. W. P. Rosenberg, Dr. D. Gawlitta
Department of Oral and Maxillofacial Surgery and Special Dental Care
University Medical Center Utrecht
Regenerative Medicine Utrecht
Utrecht University
Heidelberglaan 100, 3508 GA Utrecht, The Netherlands
E-mail: d.gawlitta@umcutrecht.nl

 The ORCID identification number(s) for the author(s) of this article can be found under <https://doi.org/10.1002/adfm.201905987>.

© 2019 The Authors. Published by WILEY-VCH Verlag GmbH & Co. KGaA, Weinheim. This is an open access article under the terms of the Creative Commons Attribution-NonCommercial License, which permits use, distribution and reproduction in any medium, provided the original work is properly cited and is not used for commercial purposes.

DOI: 10.1002/adfm.201905987

the nonwoven mats. Besides biochemical cues, the pore size is the main factor that promotes endothelialization of the luminal layer.^[7] It was suggested that to achieve a mono layer of endothelial cells, pore sizes should not be greater than the size of a cell.^[7a,8] Especially for small diameter vascular grafts, this monolayer is critical to avoid intimal hyperplasia and thrombosis.

Recently, a new fabrication technique called melt electro-writing (MEW) that employs controllable polymer melts instead of solutions has emerged.^[9] Due to the viscoelastic properties of the polymer melt, the chaotic instabilities, which occur during SES, are suppressed. The stretched polymer jet can, in combination with an automated collector plate, be used for direct writing of structures^[9d,10] composed of polymer fibers with diameters in the range of several hundreds of nanometers^[11] to micrometers.^[12] Compared to traditional additive manufacturing approaches like fused deposition modelling, the reduction in fiber diameter in combination with the control of deposition of the fibers enables generating constructs with a higher fiber density, a higher surface to volume ratio and a better control over pore architecture at a micrometer level. Using cylindrical targets and dedicated software, we have shown that it is possible with MEW to create tubular constructs with precise control over the fiber angle relative to the longitudinal axis of the tube.^[13]

Altering the fiber orientation is beneficial for the creation of biofabricated vascular grafts, as the orientation of the vSMCs and the extracellular matrix (ECM) in the tunica media is important for the contractile function of blood vessels.^[1a,3b,14] In the tunica media, collagen fibers predominately run in the circumferential direction but can also be oriented helically which is decisive for the circumferential mechanical properties of the vessel.^[15] Recapitulating the regulation of cellular orientation in the tunica media of biofabricated vascular grafts has already been the point of focus in several studies but was performed with limited control over fiber density in the selected fabrication techniques.^[14c,d,16] This often resulted in medial layers with high fiber density, lacking in space for adequate cellular interactions and resulting in slow vSMC colonization.^[16b,17]

In the native situation, cells residing in the tunica media and tunica intima have extensive crosscommunication. Therefore, a major advantage of tissue mimetic bilayered constructs is the introduction of cocultures with associated cellular crosstalk. The adequate function of a blood vessel is based on an EC monolayer that can stimulate the vSMCs by specific signaling pathways, such as the Alk1/Alk5/transforming growth factor (TGF) β pathway for steering the plastic phenotype of the vSMCs, or the secretion of nitric oxide (NO) via endothelial nitric oxide synthase for vasoconstriction and dilatation of the blood vessel.^[18] Despite its relevance, the interplay between the cell types in an engineered blood vessel are, rarely addressed. So far, most studies only have reported bilayered electrospun scaffolds supporting the culture of endothelial cells and vSM-like cells separately.^[19] Only few have shown simultaneous culturing of these cell types on bilayered tubular scaffolds in vitro^[7a,16b,20] but fall short in extensive phenotypical characterization of the cell layers and none have taken into account clinically relevant cell sources for the perspective of an eventual clinical application. To integrate that in the experiments from the beginning, the use of autologous cells, in case of vascular grafts, vSMCs, would be the best option. Still, in vitro this has

been reported as a challenge due to their limited availability and proliferative capacity, and their switch to the synthetic phenotype, which challenges clinical translation.^[21] Therefore, multipotent mesenchymal stromal cells (MSCs), which have the ability to differentiate into vSMCs are an appropriate alternative for vSMCs.^[22] Further, as a source for endothelial cells, endothelial progenitor cells (EPCs) can be used, which can also be harvested from an easily obtainable cell source (e.g., human umbilical cord blood and peripheral blood). Among the EPCs, a subgroup named “endothelial colony forming cells” (ECFCs) show high expansion potential and inherent vasculogenic and angiogenic capacity.^[23] Both, MSCs and ECFCs, can originate from autologous sources and thus are suitable for clinical translation of biofabricated vascular grafts.

Following an analysis of the architecture of a human artery, the underlying hypothesis of this study was that, if an advanced scaffold can be fabricated with tissue-mimetic layered hierarchy combined with a heterotypic topology, this scaffold can direct the formation of vessel-like cell organization, orientation, and differentiation upon seeding of ECFCs and MSCs onto the respective layers. Heterotypic topology means a basal-membrane like morphology at the inner lumen for endothelial cells and an adhesion and migration guidance for vSMCs or their progenitors in the outer layer in a tissue-analogous orientation toward the circumferential axis of the constructs. We further hypothesized that such scaffolds may result in tissue-analogous cell organization and phenotype evolution without the need for additional soluble factors or a surface bioactivation of the scaffolds.

2. Results and Discussion

Tubular scaffolds as a basis for the biofabricated vascular grafts were thus fabricated by combining SES and MEW of poly(ϵ -caprolactone) (PCL) through consecutive fiber deposition (first SES, then MEW) onto a cylindrical target with an outer diameter of 3 mm. These scaffolds were then seeded with ECFCs and MSCs. The SES nonwoven inner layer enabled the ECFCs to organize into a continuous endothelium. Furthermore, the ECFCs expressed signals associated with crosscommunication toward vSMCs. The MEW layer controlled the orientation of the MSCs, was fully populated with cells, facilitated close cell–cell contacts, and accelerated the differentiation of MSCs into vSM-like cells. Along, it was shown that the scaffold could support both cell types when cocultured, providing a platform in which cellular crosscommunication can be studied.

In order to know how to design biomimetic bilayered scaffolds with heterotypic topology, first the architecture and phenotypic aspects of a human muscular artery were established by analyzing the presence of a selection of contractile vSMC markers and associated ECM components (Figure S1, Supporting Information). Calponin, α -smooth muscle actin (α -SMA), smooth muscle myosin heavy chain (SMMHC), laminin α 5, and collagen type IV were identified and located in the natural vessel tissue (Figure S1B–F, Supporting Information). Also, overall tissue hierarchy was established (H&E staining, Figure S1A, Supporting Information). The tissue layers could be distinguished clearly, with the relatively thin tunica intima (10–20 μ m) on the luminal side of the vessel with its collagen type IV-positive basement

membrane and a fine network of connective tissue with elastic fibers. The native tissue stained positive throughout the whole thickness of the tunica media ($\approx 400 \mu\text{m}$) for the contractile vSMC and ECM markers of interest. Additionally, the vSMCs were organized in an elongated, concentric, and multilayered manner.

Based on the analysis of the human blood vessel and on the literature search presented in the introduction, design criteria for the biofabricated vascular grafts-scaffolds were formulated. The newly designed bilayered small diameter vascular grafts (3 mm \varnothing) should provide both the ECFCs and the MSCs with the appropriate environment mimicking and instructing the cells to organize and deposit matrix in the native architecture. To achieve this, we defined the following key consideration points:

1. The scaffold should provide a substrate on which the ECFCs form a continuous monolayer.
2. The endothelial monolayer should express mature EC markers, components of the basement membrane and ECM, and signals associated with crosscommunication toward vSMCs.
3. The scaffold should provide a porous outer layer that vSMCs can migrate in and fill to achieve a multilayered elongated cell organization.
4. The vSMCs should align in a near-circumferential orientation, specifically controlled by the MEW fiber orientation.
5. The scaffold should provide an environment for the MSCs to differentiate into the vSMCs contractile phenotype.

As these design criteria could not be met by any single fabrication technique, we developed a new fabrication procedure by combining two techniques, SES and MEW (Figure 1A,B). This enabled the fabrication of scaffolds with so far unachievable biomimetic and heterotypic structural features as shown in Figure 1C. The scaffolds were composed of an inner cylindrical

nonwoven ($80\% \pm 5\%$ porosity, inner diameter 3 mm) of solution electrospun PCL fibers with a diameter of $1.4 \pm 0.2 \mu\text{m}$ and a random orientation. The same material was used to create a layer of MEW fibers ($15.2 \pm 4.8 \mu\text{m}$) with a winding angle (Figures S2 and S3, Supporting Information) between 30° and 70° and controllable large open pores. As the material deposited onto the SES nonwoven by MEW was still at a temperature above its melt point, it could fuse with the fibers of the inner nonwoven as shown in Figure 1C. This is crucial to avoid delamination of the layers during cell culture and when removing the samples from the cylindrical collector they are deposited onto. As revealed via balloon inflation burst experiments, the burst pressures of the (cell-free) constructs was $2400 \pm 75 \text{ mmHg}$. This value exceeded the required pressure for transition to clinical translation based on measurements of the saphenous vein of 1700 mmHg ^[24] (Figure S4, Supporting Information).

The heterotypic electrospinning approach supported endothelialization on the inside of the dense luminal nonwoven layer as illustrated by the presence of a confluent endothelial monolayer in scaffolds with ECFC monocultures (Figure S6, Supporting Information). Importantly, this advanced scaffold design also supported so far unreached endothelialization in coculture conditions of ECFCs with MSCs (Figure 2A) and showed no infiltration of the ECFCs into the SES layer (Figure 2A and Figure S8C,D, Supporting Information). The formation of a continuous monolayer meets the achievement of key point 1. Scanning electron microscopy (SEM) demonstrated the establishment of connections between neighboring ECs (black arrows) with their extrusions (white arrows), indicative of a restrictive endothelial barrier and low permeability (Figure 2B,C). The low permeability and functional integrity of the monolayer was mostly supported by the specific

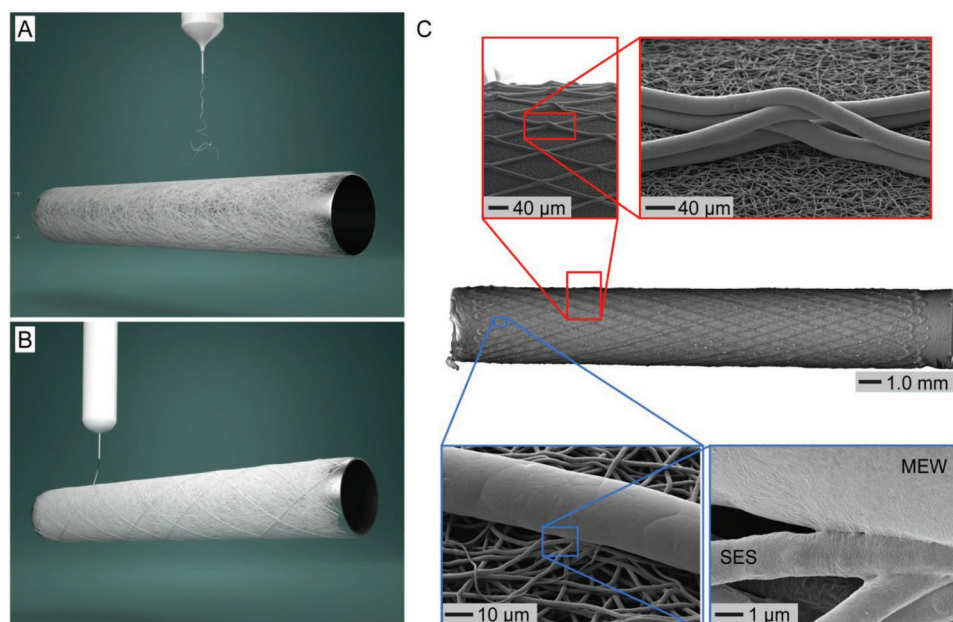


Figure 1. Preparation of bilayered tubular scaffolds. A) Solution electrospinning is used to generate a tubular nonwoven inner layer. B) The rod with the nonwoven is transferred to a melt electrowriting device and oriented fibers are deposited on top of the nonwoven luminal layer. C) The final construct is removed from the cylindrical collector. Bilayered scaffolds are made from one material and the fibers with different dimensions fuse, which prevents delamination.

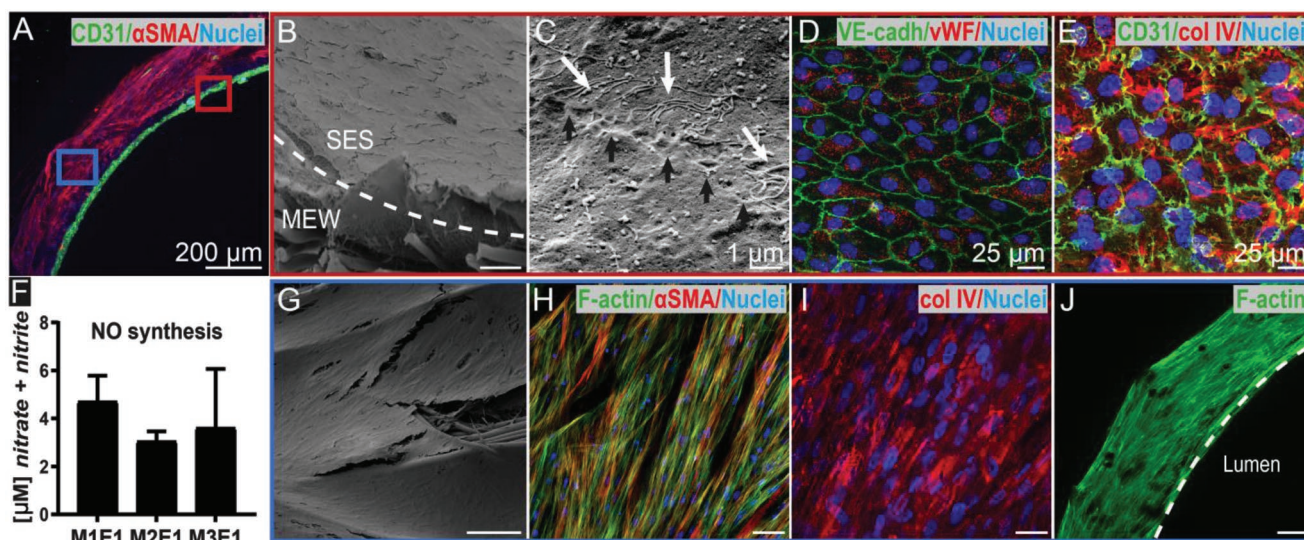


Figure 2. Cell culture on bilayered heterotypic vascular grafts. A) Layered organization and distinctive phenotypes of simultaneously cultured ECFCs (CD31⁺) and vSM-like cells (α SMA⁺) after 17 d (cross-sectional view). B) Endothelialization of the SES layer on the luminal side with C) tight cell–cell connections (black arrows) and cell extrusions (white arrows), D) positive staining for the endothelial cell markers von Willebrand factor and VE-cadherin, the latter of which was located at the cell periphery, and E) CD31; also, a collagen type IV-positive basement membrane-like matrix was detected. F) The endothelial cells produced nitric oxide (NO) for signaling to the vSM-like cells (MSC donors $n = 3$, M1–M3). G) vSM-like cells covered the medial layer in an aligned fashion, H) with elongated α SMA⁺ cells following the MEW fibers with I) a collagen type IV deposition in the direction of the cell alignment. J) vSM-like cells filled the whole thickness of the MEW layer and showed a circumferential orientation in monoculture after 7 d. Scale bars represent 100 μ m unless stated otherwise.

redistribution of the mature endothelial cell markers CD31 and vascular endothelial cadherin (VE-cadherin) toward the cell periphery (Figure 2D,E), as validated previously.^[25] The tight connections between the ECs via these interactions, are a prerequisite for an endothelium to form a semi-permeable barrier and are essential for their interaction in signaling pathways regarding endothelial plasticity, vascular integrity as well as sensing mechanical tensions, such as shear stress and to inhibit the activation of platelets and leukocytes.^[25b,26] Reproducing the functional integrity of the endothelium with barrier function is essential to resist thrombosis following introduction in vivo and is thus required to be present in biofabricated vascular grafts to pass functionality and for long term patency.^[24] The capability of the generated monocultured endothelium to prevent platelet adhesion was shown, while platelets did aggregate on the exposed scaffold surface (Figure S6D–F, Supporting Information). With this, a lining with anticoagulative properties was produced, resembling the properties of a native endothelium. Likewise, the monolayer showed positive endothelial marker staining for the platelet adhesion glycoprotein von Willebrand factor (vwF) (Figure 2D) and was supported by a collagen type IV-positive matrix (Figure 2E), as also found in the native basement membrane^[2,27] supporting the biomimetic properties of the scaffold. Expression of these EC-related markers and ECM/basement membrane components were also confirmed on a gene expression level, both in mono and cocultures (Figures S6 and S7, Supporting Information).

To meet the second key consideration point, signaling pathways for vSMC-EC communication were examined via assessment of NO secretion into the culture medium and via gene expression of the Alk1/Alk5/TGF β pathway for vSMC differentiation in cocultured biofabricated vascular grafts. For MSCs of all three donors, combined with ECFCs, the product

NO was detected in the medium (Figure 2F). Also, the presence of mRNA of the Alk1/Alk5/TGF β genes was confirmed after coculturing (Figure S7, Supporting Information). This indicated the presence of the cellular crosscommunication for vasoactivity, which is required for the development of a functional endothelium in biofabricated vascular grafts.^[24] Especially the production of NO, which is considered one of the predominant vasodilators and is involved in inhibition of platelet aggregation is necessary for a functional endothelium.^[28] The measured synthesis of NO in our culture system gives indications that the formed endothelium holds functionality and possesses the ability to signal to vSM-like cells when cultured on our biomimetic bilayered scaffolds. Altogether, the expression of the markers for mature ECs, for components of the basement membrane and ECM markers, together with the indicated presence of the cellular crosscommunication shows that also the second key consideration point was met. Further, we demonstrated that the large pores and MEW fiber alignment could induce a fast infiltration by the vSM-like cells to meet the third key consideration point in both MSC/ECFC cocultures (Figure 2J) and MSC monocultures (Figure S8, Supporting Information). The seeded MSCs covered the whole outer surface of the scaffold (Figure 2G) and appeared in an aligned fashion (Figure 2H). Moreover, the initially seeded MSCs showed the desired arrangement, indicated by the elongated cytoskeletons and α SMA-positive structures. Also collagen type IV was synthesized (Figure 2I), which was enclosing the individual vSMCs as a basement membrane-like matrix (Figure S9, Supporting Information), mimicking the native situation.^[2,27,29] To prove that the high control over MEW fiber placement could also guide the orientation of the MSCs, they were monoseeded ($n = 4$ MSC donors) on scaffolds i) without MEW layer, ii) an MEW layer with fiber winding angle of 30° (programmed

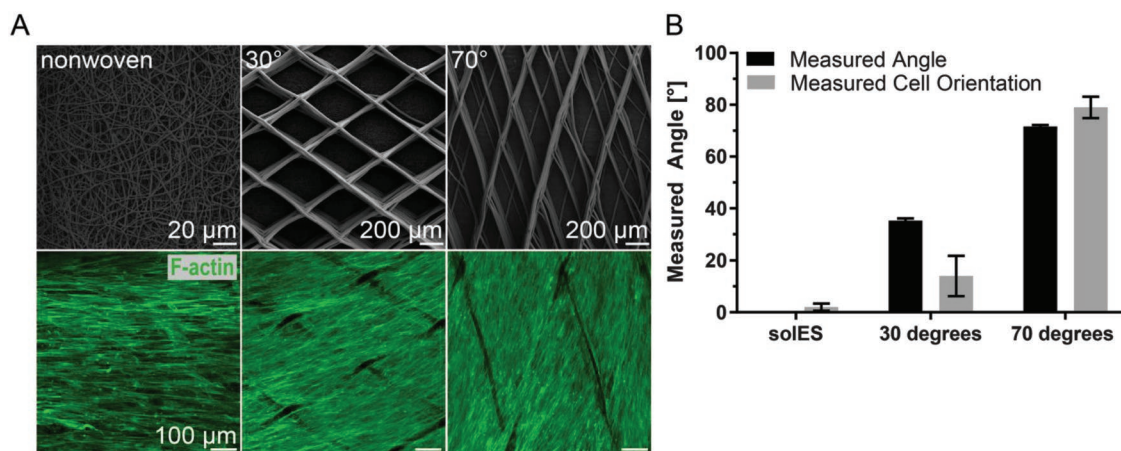


Figure 3. Influence of the orientation of melt electrospun fibers on the orientation of MSCs. A) Representative scanning electron microscopy images of the scaffolds before seeding (top row) and a projection of F-actin stained cells from a 3D stack of scaffolds after seeding and culture for 7 d (bottom row). B) The 3D projection was used to analyze the mean cell orientation throughout the thickness of the MEW layer and showed the average orientation of the melt electrospun fibers as well.

angle 30°, measured angle $35.3^\circ \pm 0.8^\circ$), and iii) samples with MEW layer at an angle of 70° (programmed angle 70°, measured angle $71.6^\circ \pm 0.6^\circ$). The cellular orientation in the whole MEW layer was analyzed based on immunofluorescence of F-actin stained cells by determining the pixel orientation of the F-actin fibers throughout the thickness of the MEW layer (Figure 3 and Figure S10 and detailed description in Supporting information). Cells seeded on the nonwoven mesh (i) were mainly oriented in the longitudinal direction of the tubular scaffold ($2.3^\circ \pm 1.4^\circ$). With increasing winding angles of the scaffold fibers, the cellular orientation changed into a near-circumferential direction (Figure 3A) as present in the native tunica media. The cells seeded on the constructs with a 70° winding angle of the MEW fibers were oriented in an angle that was larger ($77.7^\circ \pm 3.4^\circ$) than the angle of the fibers. This winding angle was used in constructs for further cell culture experiments, as this met the fourth key consideration point of (near) circumferentially arranged cells and mimicked the helically orientated collagen fibrils as in the native arteries^[14a,15a] and also the orientation of the cell nuclei of vSMC in a human aortic tunica media.^[30] Taken together, we thereby proof and verify our hypothesis that the orientation of vSMCs on tubular scaffolds can be guided in a tissue-mimetic manner by controlled orientation of fibers in the micrometer range. The open porous structure of the outer layer facilitated a fast cellular ingrowth and resulted in several layers of orientated aligned cells with close cellular interactions. We could achieve different cell orientations and found one that is potentially exploitable for facilitating vasodilation and constriction for next generation bioengineered vascular grafts.

The last key consideration point for aiming at engineering of the tunica media is to realize the SMC phenotype switch to the contractile phenotype at the proper stage during their maturation process on the scaffold. Generally, differentiation of MSCs into contractile vSMCs is accomplished by the addition of biochemical factors associated with differentiation, such as TGF- β 1 or platelet-derived growth factor subunit β .^[22d,29,31] Interestingly, we observed that by expanding bone

marrow-derived MSCs in a culture plate, supplemented with the proliferation-associated basic fibroblast growth factor (bFGF), also an induction of differentiation was observed after reaching confluency. This differentiation was accompanied by protein upregulation of the contractile vSMC marker proteins α SMA and calponin. In addition, the cells showed capacity for contraction of a collagen lattice (Figures S11A–C and S14, Supporting Information) as well as elevated gene expression levels of additional contractile vSMC markers (Figure S11D, Supporting Information). The induction of differentiation in postconfluent vSMC cultures has been reported previously^[32] and several groups showed very promising results and could, for example, use the fiber orientation to control the 2D orientation of a monolayer of vSMCs.^[33] It could be shown that the orientation, alignment and confluency can be utilized to control the phenotype of vSMCs.^[34] The effect of confluency was also reported to be existent in MSC cultures by Alimperti et al., where the induction of differentiation of MSCs into contractile vSM-like cells was described, without the use of above-mentioned differentiation growth factors.^[35] They hypothesized that the observed differentiation is a cell–cell junction-mediated process through the adherens junction cadherin-11, normally found on MSCs, with an associated autocrine action of TGF- β 1,^[35] or possibly by the secretion of a basement membrane-like matrix associated with the contractile vSMC phenotype.^[14b] In addition, the MSCs used here appeared to be positive for CD146, a marker associated with perivascular cells and were therefore more prone to vSMC differentiation (Figure S12, Supporting Information).^[36]

To more closely investigate the effect of increased cell–cell interactions on the differentiation of MSCs in our scaffold with open pores, we compared the differentiation on constructs without or with MEW layer, as the latter enhances stacking of MSCs and thereby increases cell–cell contacts in a 3D setting. To do so, we first showed that the SES layer was a sufficient substrate for the MSCs to proliferate and differentiate on, to reach the same confluency as in a culture plate, with similar expression of contractile vSMC markers on both gene and protein levels (ACTA2 – α SMA; CNN1 – Calponin; Transgelin – SM22 α

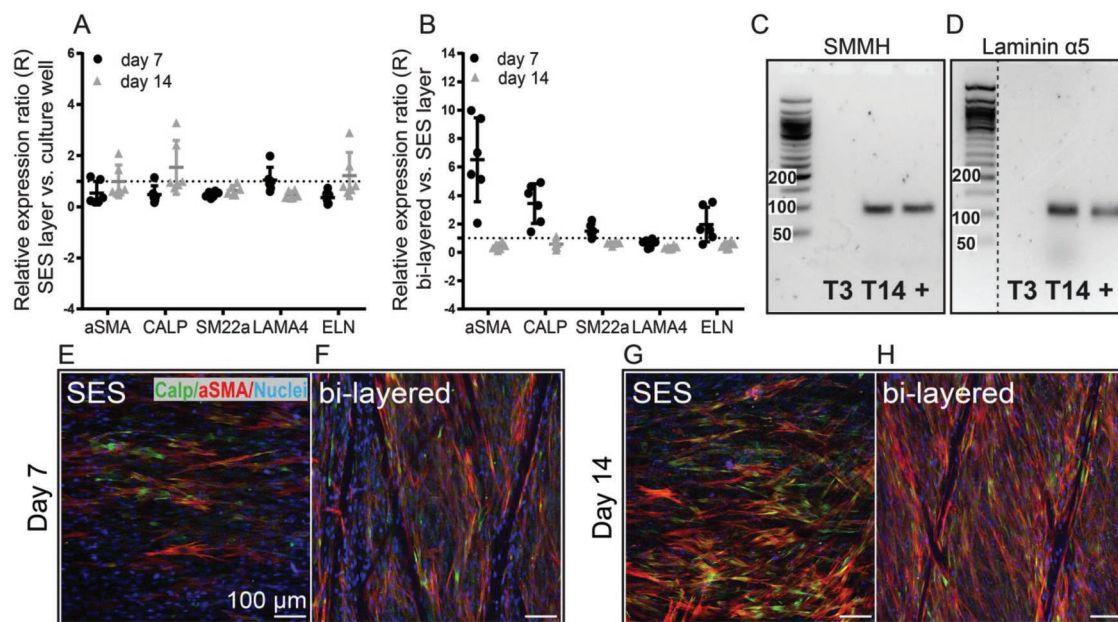


Figure 4. Confluence-driven MSC differentiation toward vSMCs. A) Similar relative gene expression levels of contractile vSMC markers of MSCs cultured on the SES only layer, compared to MSCs cultured in well plates after 7 and 14 d of culture, normalized to GAPDH. B) Comparison of gene expression levels of MSCs cultured on bilayered vascular scaffolds versus MSCs cultured on the SES only layer after 7 and 14 d of culture, normalized to GAPDH. C) qPCR product on gel electrophoresis of SMMHC, representative for both SES-only and bilayered scaffold cultures and D) laminin subunit $\alpha 5$; both (C) and (D) show qPCR products after 3 and 14 d of culture, compared to commercially obtained mature vSMCs (positive control). E) A small amount of aSMA⁺/Calponin⁺ cells on SES only scaffolds in a confluent layer after 7 d, aligned with the 0° axis, and F) in a circumferential multilayered oriented sheet on the bilayered scaffold, also with aSMA⁺/Calponin⁺ cells. G) Multilayered vSM-like cells on SES only scaffold with increased numbers of aSMA⁺/Calponin⁺ cells, compared to day 7, and H) highly organized aSMA⁺/Calponin⁺ vSM-like cells on the bilayered scaffold with elongated morphology after 14 d.

and the extracellular matrix markers LAMA4 – Laminin subunit $\alpha 4$ and ELN – Elastin) (Figure 4A, no significant differences) as found in culture plates, after both 7 and 14 d. In this setup, the MSCs were monocultured on the single-layered SES scaffold without the MEW fibers and compared to the differentiation status of MSCs cultured in plates (control group) with corresponding culture times. Accordingly, the SES proved to be a suitable substrate for culturing and differentiation (with longitudinal alignment) of MSCs into vSM-like cells in comparable rates as on a culture plate.

Next, we analyzed the influence of MEW fibers on the differentiation process of MSCs into vSM-like cells. Therefore, MSCs were monocultured and a comparison was made between the single-layered scaffold (SES only, control group) and the bilayered scaffold with the MEW fibers. After 7 d of culture, the cells on the bilayered scaffolds had higher gene expression levels of the contractile phenotype markers α SMA (6.5 ± 2.9) and calponin (3.4 ± 1.4) compared to the expression of MSCs cultured on the SES only layer (Figure 4B), though not statistically significant. The same trend could be seen on a protein level (Figure 4E,F). Additionally, the bilayered constructs contained stacked vSM-like cell sheets, composed of more aSMA⁺/Calponin⁺ cells compared to the SES only layer (Figure 4E,F and Figure S13, Supporting Information). This proves the benefit of our biomimetic scaffold design as the MEW layer provides an adjustable tool to control the phenotype of the vSM-like cells.

The differences in gene expression between the bilayered scaffold and the single SES layer were not present anymore

after 14 d. This could be explained by the slower proliferation of vSM-like cells on the SES only layer (Figure 4B) between days 7 and 14, meaning that the induction of confluency-induced differentiation has a delay compared to the bilayered seeded scaffold. This was confirmed by the rapid establishment of 3D stacked cell sheets and associated differentiation of the MSCs in the bilayered graft by day 7 already (Figure 4E,F). At both the early and late time points, comparable levels of relative gene expression of SM22a (1.5 ± 0.5), tropo(elastin) (2.0 ± 1.2), and LAMA4 (0.6 ± 0.3) were found in both groups. Overall, more aSMA⁺/Calponin⁺ cells were present in the bilayered scaffolds compared to the SES only scaffold. Thus, in addition to the previously shown beneficial effect of the MEW layer on the vSM-like orientation, the MEW fibers also seem to provide a substrate for the cells to attach to and proliferate faster into a 3D differentiated stack of cells. This is in comparison to the, in general single layer of, vSM-like cells on the SES scaffold. Importantly, all vSMC markers were also present in the cocultured constructs (Figure S7, Supporting Information). Taken together, these data evidence that our tissue-mimetic scaffold design with heterotypic morphology, achieved through conversion of SES and MEW onto cylindrical targets, provided an open-porous 3D microenvironment for the MSCs that induced differentiation into the contractile phenotype, proving that the fifth and final key point was met.

To evaluate if the MSCs indeed acquired an actual vSMC phenotype, we included a broad pool of markers related to the contractile SMC phenotype (double positive aSMA⁺/calponin⁺ cells

and SM22 α), together with relevant ECM components (collagen type IV, laminin subunit $\alpha 4$ and (tropo)elastin). Noteworthy, analysis of only expression of calponin or α SMA as smooth muscle cell markers may fail to indicate the true differentiation state of MSCs, as nondifferentiated MSCs and myofibroblasts have the capability to simultaneously express some of the vSMC contractile phenotype markers.^[37] As such, in this study, the detection of α SMA/calponin-double positive cells was assessed, since these are most likely representing true vSMC cells, as previously reported by Liu et al.¹ To further explore the true differentiation state of the MSCs toward vSM-like cells, two markers associated with the highest degree of vSMC differentiation specificity were selected to additionally confirm their fate by polymerase chain reaction (PCR). These were SMMHC, considered to be the most selective vSMC marker^[21] and laminin $\alpha 5$ (laminin-511 and/or 521), normally found in the basement membrane of mature vSMCs.^[29] MSCs cultured on the SES-only scaffold and bilayered scaffold for 14 d (T14) expressed SMMHC, while this was absent after only 3 d (T3) of culture (Figure 4C,D). Likewise, the vSM-like cells were found to express the laminin $\alpha 5$ subunit (Figure 4C,D). In addition, the potential for contraction of the vSM-like cells was confirmed in a collagen gel lattice contraction assay (Figure S14, Supporting Information). Hence, the expression of markers of the contractile vSMC phenotype in the biofabricated vascular grafts, their capacity for gel contraction, and in addition, the observations for the elongated morphology of the smooth muscle (SM)-like cells, are reliable indicators of a smooth muscle cell-like phenotype differentiated from MSCs.

3. Conclusion

In conclusion, a new hybrid fabrication procedure was developed by combining two techniques, solution electrospinning and MEW. This allows for a tissue-structure guided fabrication of heterotypic bilayered tubular scaffolds in a two-step approach with one order of magnitude difference in fiber thickness, within the same scaffold. The achieved tubular scaffold architecture resembled the dimensions and spatial organization of the intimal and medial layers of a native vessel. Thereby, the scaffolds were directing cell morphology and differentiation. The inner SES layer supported the formation of a confluent endothelium, with indications of a restrictive endothelial barrier function with low cellular permeability. The open-porous outer MEW layer with a low fiber density and controlled deposition and orientation was the fundament for a fast vSM-like cell colonization in an orientated 3D manner. The heterotypic scaffold design tackles, for the first time, the problems generally described with electrospinning of tubular scaffolds for the mimicry of the tunica media. Importantly, the five key consideration points were achieved with cocultures on the bilayered vascular graft and showed the correct phenotypes after cellular characterization. Also, the in vitro functionality of the endothelium was proven by its anticoagulative potential and with the synthesis of NO, indispensable for the communication between the two cell layers. Finally, we want to emphasize that neither soluble factors nor a surface functionalization of the scaffolds was needed for achieving these results, underlining that

heterotypic scaffold design that offers biomimetic morphology for more than one cell type within one construct, is a powerful trigger for biofabrication of tissue analogues.

The translation into the application, which includes mechanical optimization of the constructs and further maturation of the cellular phenotypes, is the focus of ongoing studies where the technology is extrapolated to more compliant polymers and where hemodynamic forces stimulate the maturation, to ultimately direct the evolution of a functional vascular graft into a neovessel. Future work will also explore whether the heterotypic design can be exploited to also modulate the immune response toward a regenerative one.

4. Experimental Section

Additional materials and methods can be found in the Supporting Information.

Scaffold Fabrication—Solution Electrospinning: Prior to electrospinning, 210 mg PCL (Purasorb PC12, Mn 57 kDa, measured in chloroform against a poly(methyl methacrylate) standard, Corbion, Netherlands) was dissolved in 0.9 mL of hexafluoroisopropanol (Sigma) for 12 h in an incubator at 37 °C and transferred into a syringe (1 mL, BBraun) equipped with a flat-tipped hypodermic needle (27G needle, Stericam, BBraun). Solution electrospinning was performed with a setup composed of a syringe pump (wpi Ltd), a grounded rotating collector, and a high voltage source. The high voltage (12 kV) was applied to the needle tip and the fibers were collected onto a rotating cylindrical target with a diameter of 3 mm and a length of 20 cm placed in a distance of 18 cm from the charged nozzle. The feed rate of the dissolved PCL was 0.5 mL h⁻¹ and spinning was performed for 14 min per mandrel while rotating the mandrel at 120 rpm.

Scaffold Fabrication—Melt Electrowriting: The nonwoven mesh still attached to the cylindrical collector was transferred to the custom-made melt electrowriting device for further processing. The same polymer as used for solution electrospinning was molten (89 °C) in a syringe equipped with a flat tipped spinneret (22G, Precision needle, Nordson EFD) and dispensed with a pressure of 0.7 bar. A voltage of 4.57 kV was applied to the tip and the nozzle was placed with a distance of 4 mm above the nonwoven mesh. Combining rotation and translation of the collector, PCL fibers could be deposited onto the solution electrospun layer with a predefined winding angle. After melt electrowriting the samples were removed from the collector for further processing.

Scaffold Characterization (SEM/Porosity): The scaffolds were sputter coated with an 8 nm platinum coating (EM ACE600, Leica) and analyzed via SEM (Crossbeam 340, Carl Zeiss). The winding angle, the diameter of the solution electrospun, and the melt electrowritten fibers were measured based on the images using imagej at ten different locations, respectively. The porosity of the solution electrospun nonwoven meshes was analyzed at the European Synchrotron Radiation Facility using the ID19 beamline with a voxel size of 0.16 μ m. The data were processed using imagej to calculate the porosity of the scaffolds.

Mechanical Testing: Mechanical testing of the scaffolds with a 70° winding angle was performed with a mechanical tester (Z010, Zwick/Roell) using a 100 N load cell. The burst pressure was analyzed using balloon catheters (UROMED) with an initial diameter of 2.7 mm. The burst pressure was detected with a manometer (N = 5).

Scaffold Seeding: Bilayered scaffolds and SES-only scaffolds were gamma-sterilized, cut in pieces of \approx 3 mm in length and immersed in 70% ethanol followed by three times washing in phosphate-buffered saline (PBS). To promote protein absorption, scaffolds were immersed in medium with 10% FBS for at least 3 h at 37 °C, prior to cell seeding. Next, cells (see the Supporting Information) were seeded on the scaffold with a density of 8000 cells mm⁻² (cell suspension concentration 12 \times 10⁶ cells mL⁻¹ for MSCs and 24 \times 10⁶ cells mL⁻¹ for ECFCs), for 1 h at 37 °C, resulting in \approx 120 000 seeded cells per scaffold. The

seeding efficiency of both the ECFCs ($46.09 \pm 12.21\%$) and MSCs ($55.64 \pm 13.31\%$) was determined via DNA quantification of seeded scaffolds after 16 h, compared to 100% of seeded cells (Figure S5, Supporting Information). For cell seeding, three groups were made: i) scaffolds monoseeded with MSCs on the outer layer (group M), ii) scaffolds seeded with ECFCs into the luminal side (group E), or iii) coseeded scaffolds with ECFCs and MSCs (group ME). Seeding was performed as follows: for group M (i), the scaffolds were placed horizontally on a sterile petridish and 1/4th of the total cell amount was pipetted on each quarter. Scaffolds were rotated 1/4th every 15 min. For group E (ii), the total amount of ECFCs was seeded inside the, with medium filled, lumen and immediately rotated to distribute the cell suspension. Hereafter, the scaffolds were rotated 1/4th every 15 min. For the cocultured group ME (iii), 14 d cultured scaffolds from group M (i) were placed in a petridish and were seeded with ECFCs as described for group E till day 17 (ii). To confirm reproducibility, groups M (i) and group ME (iii) had independent biological replicates with $n = 4$ or $n = 3$ different MSC donors respectively (MSC1–4), together with experimental duplicates ($n = 2$) for each outcome parameter. One donor of the ECFC was used in all experiments.

Scaffold Cultures: All groups were vertically cultured in 48-well cultured plates with 0.5 mL of the desired medium. Group M (ii) was cultured in MSC expansion medium (α -Minimum Essential Medium, 10% heat-inactivated FBS, PenStrep, ascorbic acid-2-phosphate, and 1 ng mL⁻¹ bFGF) for 7 or 14 d. Group E (ii) and group ME (iii) were cultured in endothelial cell growth medium 2 and cultured for (ii) 7 and (iii) 17 d (14 d MSC monoculture in MSC expansion medium, followed by 3 d coculturing). After culture time, the discs were either fixed in 10% Formalin solution or 6% glutaraldehyde (for SEM), or used for RNA isolation. For MSC control situations, MSC1 was cultured in a 12 wells culture-plate (seeding density 1500 cells cm⁻²) for 3, 7, or 14 d in MSC expansion medium, supplemented with 1 ng mL⁻¹ bFGF, after which the monolayer was either fixed or used for RNA isolation.

SEM of Cell-Seeded Scaffolds: Scaffolds were washed in PBS and fixed in 6% glutaraldehyde in PBS (25% in H₂O, G6257, Sigma-Aldrich) on ice, for 15 min. Next, samples were washed twice with PBS on ice for 10 min, after which the samples were dehydrated at room temperature, each step for 10 min ($2 \times 70\%$, $2 \times 90\%$, $2 \times 100\%$). Afterward, samples were incubated twice with hexamethyldisilazane (440191, Sigma-Aldrich) for 15 min and air dried afterward. After the fixation, scaffolds were sputter-coated with a platinum coating (4 nm, EM ACE600, Leica) and analyzed via SEM (Crossbeam 340, Carl Zeiss).

Orientation of the vSM-Like Cells: To assess the influence of the winding angle on the orientation of the MSCs, whole mount immunofluorescent staining was performed for F-actin (Sigma, Phalloidin Fluorescein Isothiocyanate labeled; P5282, 0.2×10^{-6} M) on group M (i), after 7 d, with varying winding angles (no MEW layer— 30° – 70°). Of every scaffold with specific winding angle, seeding was independently repeated with four different MSC donors (MSC1–4) ($n = 2$) to confirm reproducibility. Confocal microscopy (Leica DMi8) was used for imaging. 3D Z-stacks were made from the outer MEW layer of three locations per sample, Z-stack settings were set for every sample individually but with the same amount of images (21) for all samples. Maximum projections were made with ImageJ 1.47v and converted into 8-bit followed by loading in the orientation plugin (min. coherency 80% – min. energy 10%). Orientation of the cells were quantified in the maximum projections of the 3D stacks made from the total MEW layer (P1) only the bottom (P2) or only the upper (P3) zone of the MEW layer. Graph 1 in Figure 3 shows values of P1 (no difference was found between P1–P2–P3).

Fluorescent Stainings—ECM and Vascular Smooth Muscle Cell Markers: To demonstrate that the seeded MSCs and their extra cellular matrix showed a vSMC phenotype, fixed samples were cut in smaller pieces, permeabilized (15 min in 0.2% Triton-X/PBS), and blocked (15 min in 5% bovine serum albumin in PBS) for nonspecific protein binding. Primary antibodies for Laminin subunit $\alpha 5$ (clone 4B12, MABT39, Merck Millipore 0.015 mg mL⁻¹) and Collagen IV (ab769 Millipore, 0.04 mg mL⁻¹) were incubated for 1 h at room temperature (with matched isotype controls). Washing steps were performed with 0.1% Tween in

tris-buffered saline (TBS), after which the matching secondary antibody incubation (α M Alexa 546 or α G, life technologies 4 μ g mL⁻¹; α G Alexa 546, Life Technologies, 2 μ g mL⁻¹) was carried out for 1 h at room temperature. Calponin (CALP, MU333-UC, Biogenex, 0.15 mg mL⁻¹) staining was performed with the avidin–biotin complex (ABC) method, with sheep antimouse biotinylated (1:300, RPN1001v1, GE Healthcare) as secondary antibody and as tertiary antibody Streptavidin, Alexa Fluor 488 Conjugate (S32354, Life technologies, 0.005 mg mL⁻¹), together with α -SMA (Clone 1A4, Cy3 0.5 μ g mL⁻¹, C6198, Sigma-Aldrich) for costaining. Nuclei were counterstained with 4',6-diamidino-2-phenylindool 100 ng mL⁻¹ (DAPI, Sigma) for 15 min and washed with PBS and visualized by confocal imaging (Leica DMi8).

Fluorescent Stainings—Endothelial Markers: To demonstrate that the seeded ECFCs contained the endothelial phenotype in the monolayer, immunofluorescence staining for CD31 (0.13 mg mL⁻¹ mouse antihuman CD31, M0823, Dako) (ABC method and antibodies as described above), vWF (3E2D10, Abcam 194405, 0.5 μ g mL⁻¹), and VE-cadherin (D87F2, Cell signal, 2500S, 1:250) was conducted. After permeabilization, nonspecific protein binding was blocked followed by 1 h of incubation with the primary antibodies. After washing with 0.1% Tween in TBS, 1 h of incubation with the secondary antibodies, α M Alexa 546 life technologies - A-11003, 0.004 mg mL⁻¹, or α R HiLyte Fluor 488, 0.001 mg mL⁻¹, respectively, was performed. Finally, nuclei were counterstained with e (DAPI staining 100 ng mL⁻¹ (Sigma)) for 15 min at room temperature. Staining was visualized by confocal imaging (Leica DMi8).

Gene Expression—RNA Isolation: Total cellular RNA was extracted by resuspending in 0.5 mL Trizol Reagent (Thermo Fisher Scientific) for 5 min at room temperature. Samples were stored at -80°C till further use. RNA was isolated from the samples by mixing the RNA extraction in Trizol with 20% chloroform (Millipore) and incubating for 3 min at room temperature. Tubes were centrifuged at $12.000 \times g$ for 15 min (4°C) after which the colorless upper aqueous phase was pipetted off and mixed with an equal amount of mL 2-propanol (Sigma) (≈ 0.25 mL) and 0.5 μ L glycogen (R0551, Thermo Fisher Scientific). This mixture was incubated for 10 min at room temperature and followed by centrifugation at $12.000 \times g$ for 10 min (4°C). Then, the pellet was washed in 75% ethanol and centrifuged at $7.500 \times g$ for 5 min (4°C). The ethanol was aspirated and the pellet was air dried. Afterward, the pellet was resuspended in 10 μ L of RNase-free water and heated to 55°C for 10 min, shortly vortexed and put on ice. A DNase step was performed by addition of 1 μ L of Turbo DNase buffer (AM2238, Ambion) and 0.5 μ L DNase (2 U μ L⁻¹) per samples, 30 min incubation at 37°C and inactivation for 10 min at 75°C .

Gene Expression—Quantitative real-time (RT)-PCR: For use in the qPCR, total RNA was first reverse-transcribed into cDNA by means of a iScript cDNA synthesis kit (Biorad, 170-8890). The RNA input concentration was set to the sample with the lowest yield (0.5 μ g), providing the same cDNA end-concentration for all samples used in this data set. The synthesis reaction was performed according to the manufacturer's instruction under the following cycling conditions: 25°C for 5 min, 30 min at 42°C , 5 min at 85°C , and hold at 4°C . The cDNA product was then diluted till an end-concentration of 5 ng μ L⁻¹ with RNase-free water and stored at -80°C till further use.

The qPCR reaction mix was prepared with the FastStart SYBR green master (Sigma, 04673484001) for a reaction volume of 20 μ L with 10 ng of cDNA and 500×10^{-9} M per primer (forward and reversed). The qPCR reaction was performed in a Roche LightCycler 96, according to the manufacturer's instruction under the following cycling conditions: Preincubation at 95°C for 5 min, three-step amplification (50 cycles) of 10 s 95°C /15 s at 60 or 63°C /30 s at 72°C .

Samples from group M (i) and group ME (iii) were checked for the quantitative expression of mRNA of SMC-specific genes, including α SMA, CALP, Smooth Muscle 22 α (SM22 α), and MY11 (SMMHC); mature endothelial specific genes, including CD31, VE-cadherin, vWF; ECM specific genes associated with vSMC maturation and basal membrane formation, including Laminin subunit $\alpha 4$ and $\alpha 5$ and (tropo) elastin; and/or genes involved in EC-vSMC crosscommunication,

including TGF β and its opposing Activin receptor-like kinase type 1 and 5 receptor of the Smad pathways. The most optimal housekeeping gene among a set of candidates was selected according to its expression stability. The algorithm from Normfinder indicated that the optimal normalization gene for this data set was glyceraldehyde-3-phosphate dehydrogenase (GAPDH). Primer sequence and temperature can be found in Table S1 in the Supporting Information.

Gene Expression—Relative Gene Expression: For group M (i), comparisons were made for day 3–7–14 for MSCs cultured in a wells plate (control situation 1), cultured on the SES only layer (test situation 1 and control situation 2) and MSCs cultured on the bilayered scaffold (test situation 2). Relative gene expression was calculated including an efficiency correction for real-time PCR efficiency of the individual transcripts.^[38,39]

$$\text{Ratio} = \left(E_{\text{target}} \right)^{\Delta C P_{\text{target}(\text{control}-\text{sample})}} / \left(E_{\text{ref}} \right)^{\Delta C P_{\text{ref}(\text{control}-\text{sample})}} \quad (1)$$

With this, relative gene expression values above 1 indicate higher expression of the mRNA in the samples compared to the control situation. Conversely, relative expression values below 1 indicate less mRNA in the experimental group versus control group. For group ME (iii), no comparisons were made to avoid influence of varying ratios of the cell-types in the cocultured constructs, especially when comparing to monocultures; instead, gel electrophoresis of the qPCR product is shown.

Gene Expression—Gel Electrophoresis: Sample groups (group M) with minimal amounts of target nucleic acid (Ct values between 38 and 42) were checked for amplification of the true sequence of interest by analyzing the fragment length via gel electrophoresis. In short, a 3% agarose solution was prepared in Tris/Borate/ethylenediamine tetraacetic acid buffer with 0.01 $\mu\text{L mL}^{-1}$ sybersafe solution. The qPCR end products of interest (and corresponding negative qPCR primer control H₂O) were prepared with gel loading dye (Purple (6X), no sodium dodecyl sulfate, New England Biolabs (NEB) B7025). Slots in the solidified gel were filled with 12 μL of prepared sample volume or 1 μg of the ladder in loading dye (50 bp DNA ladder, NEB N3236S). Images were made with a biorad UV gel reader in the program Quantity One 4.5.2, after running for 45 min on 80 Volts at RT.

Image Adaptions: Images obtained with confocal microscopy (Leica DMi8SP8x) were adjusted with Adobe Photoshop CS6 for intensity of the signal by removing under and overexposed pixels. No local thresholding was performed. Confocal laser power was kept the same within each session and when comparing samples. Images from gel electrophoresis, made with Quantity One 4.5.2, were cropped in Adobe Photoshop CS6 and contrast was adjusted accordingly.

Statistical Analysis: The statistical analysis was performed with the software package Statistica 13 (TIBICO Software Inc.). A *t*-test was performed on the effective $E\Delta C P$ values ($(E_{\text{target}})\Delta C P_{\text{target}(\text{control}-\text{sample})}$ vs $(E_{\text{ref}})\Delta C P_{\text{ref}(\text{control}-\text{sample})}$) of the gene expression to evaluate if the data from the qPCR measurements show a statistically relevant difference from the house keeping gene, both normalized to the control group.

Supporting Information

Supporting Information is available from the Wiley Online Library or from the author.

Acknowledgements

T.J. and I.P. contributed equally to this work. This research was partially supported by an NWO (Netherlands Organization for Scientific Research) Graduate Program Grant (022.005.018) and by the European Research Council (Grant No. 617989 Design2Heal). The authors thank Simon Zabler for help with the nanocomputed tomography

measurements and Daimon Hall (carbonandneon.com) for support with graphical design.

Conflict of Interest

The authors declare no conflict of interest.

Keywords

biofabricated vascular graft, heterotypic scaffold design, hybrid fabrication, melt electrowriting (MEW), primary vascular smooth muscle-like cells (vSMCs)

Received: July 23, 2019

Published online: August 16, 2019

- [1] a) A. Hasan, A. Memic, N. Annabi, M. Hossain, A. Paul, M. R. Dokmeci, F. Dehghani, A. Khademhosseini, *Acta Biomater.* **2014**, *10*, 11; b) S. Ravi, Z. Qu, E. L. Chaikof, *Vascular* **2009**, *17*, S45.
- [2] L. F. Yousef, J. Di Russo, L. Sorokin, *Cell Adhes. Migr.* **2013**, *7*, 101.
- [3] a) D. G. Seifu, A. Purnama, K. Mequanint, D. Mantovani, *Nat. Rev. Cardiol.* **2013**, *10*, 410; b) N. Thottappillil, P. D. Nair, *Vasc. Health Risk Manage.* **2015**, *11*, 79; c) S. Ravi, E. L. Chaikof, *Regener. Med.* **2010**, *5*, 107.
- [4] a) N. L'Heureux, S. Paquet, R. Labbe, L. Germain, F. A. Auger, *FASEB J.* **1998**, *12*, 47; b) N. L'Heureux, N. Dusserre, G. Konig, B. Victor, P. Keire, T. N. Wight, N. A. Chronos, A. E. Kyles, C. R. Gregory, G. Hoyt, R. C. Robbins, T. N. McAllister, *Nat. Med.* **2006**, *12*, 361.
- [5] a) B. C. Isenberg, C. Williams, R. T. Tranquillo, *Circ. Res.* **2006**, *98*, 25; b) Z. Syedain, J. Reimer, M. Lahti, J. Berry, S. Johnson, R. T. Tranquillo, *Nat. Commun.* **2016**, *7*, 12951; c) K. T. Morin, J. L. Dries-Devlin, R. T. Tranquillo, *Tissue Eng., Part C* **2014**, *20*, 553; d) S. Koch, T. C. Flanagan, J. S. Sachweh, F. Tanius, H. Schnoering, T. Deichmann, V. Ella, M. Kellomaki, N. Gronloh, T. Gries, R. Tolba, T. Schmitz-Rode, S. Jockenhoewel, *Biomaterials* **2010**, *31*, 4731; e) B. Tschoeke, T. C. Flanagan, S. Koch, M. S. Harwoko, T. Deichmann, V. Ella, J. S. Sachweh, M. Kellomaki, T. Gries, T. Schmitz-Rode, S. Jockenhoewel, *Tissue Eng., Part A* **2009**, *15*, 1909.
- [6] a) K. A. Rocco, M. W. Maxfield, C. A. Best, E. W. Dean, C. K. Breuer, *Tissue Eng., Part B* **2014**, *20*, 628; b) E. Ercolani, C. Del Gaudio, A. Bianco, *J. Tissue Eng. Regener. Med.* **2015**, *9*, 861.
- [7] a) Y. M. Ju, J. S. Choi, A. Atala, J. J. Yoo, S. J. Lee, *Biomaterials* **2010**, *31*, 4313; b) B. M. Whited, M. N. Rylander, *Biotechnol. Bioeng.* **2014**, *111*, 184; c) D. Narayan, S. S. Venkatraman, *J. Biomed. Mater. Res., Part A* **2008**, *87A*, 710.
- [8] Y. Zhang, H. Ouyang, C. T. Lim, S. Ramakrishna, Z. M. Huang, *J. Biomed. Mater. Res.* **2005**, *72B*, 156.
- [9] a) T. Jungst, M. L. Muerza-Cascante, T. D. Brown, M. Standfest, D. W. Huttmacher, J. Groll, P. D. Dalton, *Polym. Int.* **2015**, *64*, 1086; b) T. D. Brown, P. D. Dalton, D. W. Huttmacher, *Prog. Polym. Sci.* **2016**, *56*, 116; c) T. D. Brown, P. D. Dalton, D. W. Huttmacher, *Adv. Mater.* **2011**, *23*, 5651; d) T. D. Brown, A. Slotosch, L. Thibaudeau, A. Taubenberger, D. Loessner, C. Vaquette, P. D. Dalton, D. W. Huttmacher, *Biointerphases* **2012**, *7*, 13.
- [10] P. D. Dalton, N. T. Joergensen, J. Groll, M. Moeller, *Biomed. Mater.* **2008**, *3*, 034109.
- [11] G. Hochleitner, T. Jungst, T. D. Brown, K. Hahn, C. Moseke, F. Jakob, P. D. Dalton, J. Groll, *Biofabrication* **2015**, *7*, 035002.

- [12] A. Hrynevich, B. S. Elci, J. N. Haigh, R. McMaster, A. Youssef, C. Blum, T. Blunk, G. Hochleitner, J. Groll, P. D. Dalton, *Small* **2018**, *14*, 1800232.
- [13] E. McColl, J. Groll, T. Jungst, P. D. Dalton, *Mater. Des.* **2018**, *155*, 46.
- [14] a) N. J. Driessen, W. Wilson, C. V. Bouten, F. P. Baaijens, *J. Theor. Biol.* **2004**, *226*, 53; b) U. Hedin, J. Roy, P. K. Tran, K. Lundmark, A. Rahman, *Thromb. Haemostasis* **1999**, *82*, 23; c) Y. Wang, H. Shi, J. Qiao, Y. Tian, M. Wu, W. Zhang, Y. Lin, Z. Niu, Y. Huang, *ACS Appl. Mater. Interfaces* **2014**, *6*, 2958; d) M. Zhu, Z. Wang, J. Zhang, L. Wang, X. Yang, J. Chen, G. Fan, S. Ji, C. Xing, K. Wang, Q. Zhao, Y. Zhu, D. Kong, L. Wang, *Biomaterials* **2015**, *61*, 85.
- [15] a) A. H. Huang, L. E. Niklason, *Cell. Mol. Life Sci.* **2014**, *71*, 2103; b) J. M. Caves, V. A. Kumar, A. W. Martinez, J. Kim, C. M. Ripberger, C. A. Haller, E. L. Chaikof, *Biomaterials* **2010**, *31*, 7175.
- [16] a) A. Agrawal, B. H. Lee, S. A. Irvine, J. An, R. Bhuthalingam, V. Singh, K. Y. Low, C. K. Chua, S. S. Venkatraman, *Int. J. Biomater.* **2015**, *2015*, 1; b) Y. M. Ju, H. Ahn, J. Arenas-Herrera, C. Kim, M. Abolbashari, A. Atala, J. J. Yoo, S. J. Lee, *Acta Biomater.* **2017**, *59*, 58; c) B. Yuan, Y. Jin, Y. Sun, D. Wang, J. Sun, Z. Wang, W. Zhang, X. Jiang, *Adv. Mater.* **2012**, *24*, 890.
- [17] a) S. Deepthi, M. Nivedhitha Sundaram, P. Vijayan, S. V. Nair, R. Jayakumar, *Int. J. Biol. Macromol.* **2018**, *109*, 85; b) J. Nam, Y. Huang, S. Agarwal, J. Lannutti, *Tissue Eng.* **2007**, *13*, 2249.
- [18] a) M. J. Goumans, G. Valdimarsdottir, S. Itoh, F. Lebrin, J. Larsson, C. Mummery, S. Karlsson, P. ten Dijke, *Mol. Cell* **2003**, *12*, 817; b) Y. Zhang, T. S. Lee, E. M. Kolb, K. Sun, X. Lu, F. M. Sladek, G. S. Kassab, T. Garland, Jr., J. Y. Shyy, *Arterioscler., Thromb., Vasc. Biol.* **2006**, *26*, 1281.
- [19] a) S. H. Lim, S. W. Cho, J. C. Park, O. Jeon, J. M. Lim, S. S. Kim, B. S. Kim, *J. Biomed. Mater. Res., Part B* **2008**, *85B*, 537; b) D. Liu, T. Xiang, T. Gong, T. Tian, X. Liu, S. Zhou, *ACS Appl. Mater. Interfaces* **2017**, *9*, 19725; c) X. Liu, J. Wang, F. Dong, P. Song, H. Li, Y. Hou, *J. Biomater. Appl.* **2017**, *32*, 219.
- [20] a) K. H. Nakayama, P. A. Joshi, E. S. Lai, P. Gujar, L. M. Joubert, B. Chen, N. F. Huang, *Regener. Med.* **2015**, *10*, 745; b) L. Ye, J. Cao, L. Chen, X. Geng, A. Y. Zhang, L. R. Guo, Y. Q. Gu, Z. G. Feng, *J. Biomed. Mater. Res., Part A* **2015**, *103*, 3863; c) Y. Liu, J. Lu, H. Li, J. Wei, X. Li, *Acta Biomater.* **2015**, *11*, 114.
- [21] G. K. Owens, *Physiol. Rev.* **1995**, *75*, 487.
- [22] a) M. Abedin, Y. Tintut, L. L. Demer, *Circ. Res.* **2004**, *95*, 671; b) S. Gojo, N. Gojo, Y. Takeda, T. Mori, H. Abe, S. Kyo, J. Hata, A. Umezawa, *Exp. Cell Res.* **2003**, *288*, 51; c) K. K. Hirschi, M. W. Majesky, *Anat. Rec.* **2004**, *276A*, 22; d) Z. Gong, G. Calkins, E. C. Cheng, D. Krause, L. E. Niklason, *Tissue Eng., Part A* **2009**, *15*, 319; e) Z. Gong, L. E. Niklason, *FASEB J.* **2008**, *22*, 1635.
- [23] a) K. K. Hirschi, D. A. Ingram, M. C. Yoder, *Arterioscler., Thromb., Vasc. Biol.* **2008**, *28*, 1584; b) D. A. Ingram, L. E. Mead, H. Tanaka, V. Meade, A. Fenoglio, K. Mortell, K. Pollok, M. J. Ferkowicz, D. Gilley, M. C. Yoder, *Blood* **2004**, *104*, 2752.
- [24] M. B. Chan-Park, J. Y. Shen, Y. Cao, Y. Xiong, Y. Liu, S. Rayatpisheh, G. C. Kang, H. P. Greisler, *J. Biomed. Mater. Res., Part A* **2009**, *88A*, 1104.
- [25] a) S. M. Albelda, W. A. Muller, C. A. Buck, P. J. Newman, *J. Cell Biol.* **1991**, *114*, 1059; b) J. Gavard, *Cell Adhes. Migr.* **2014**, *8*, 158.
- [26] P. Lertkiatmongkol, D. Liao, H. Mei, Y. Hu, P. J. Newman, *Curr. Opin. Hematol.* **2016**, *23*, 253.
- [27] F. Arends, C. Nowald, K. Pflieger, K. Boettcher, S. Zahler, O. Lieleg, *PLoS One* **2015**, *10*, e0118090.
- [28] M. Khazaei, F. Moien-Afshari, I. Laher, *Pathophysiology* **2008**, *15*, 49.
- [29] T. Seeger, M. Hart, M. Patarroyo, B. Rolauffs, W. K. Aicher, G. Klein, *PLoS One* **2015**, *10*, e0137419.
- [30] a) G. A. Holzapfel, T. C. Gasser, M. Stadler, *European Journal of Mechanics - A/Solids* **2002**, *21*, 441; b) B. Spronck, R. T. Megens, K. D. Reesink, T. Delhaas, *Biomech. Model. Mechanobiol.* **2016**, *15*, 419.
- [31] a) W. Gu, X. Hong, A. Le Bras, W. N. Nowak, S. Issa Bhaloo, J. Deng, Y. Xie, Y. Hu, X. Z. Ruan, Q. Xu, *J. Biol. Chem.* **2018**, *293*, 8089; b) J. A. Beamish, P. He, K. Kottke-Marchant, R. E. Marchant, *Tissue Eng., Part B* **2010**, *16*, 467.
- [32] A. S. Rovner, R. A. Murphy, G. K. Owens, *J. Biol. Chem.* **1986**, *261*, 14740.
- [33] a) J. Zhong, H. Zhang, J. Yan, X. Gong, *Colloids Surf., B* **2015**, *136*, 772; b) H. Yuan, J. Qin, J. Xie, B. Li, Z. Yu, Z. Peng, B. Yi, X. Lou, X. Lu, Y. Zhang, *Nanoscale* **2016**, *8*, 16307.
- [34] a) Y. Cao, Y. F. Poon, J. Feng, S. Rayatpisheh, V. Chan, M. B. Chan-Park, *Biomaterials* **2010**, *31*, 6228; b) J. Y. Shen, M. B. Chan-Park, B. He, A. P. Zhu, X. Zhu, R. W. Beuerman, E. B. Yang, W. Chen, V. Chan, *Tissue Eng.* **2006**, *12*, 2229.
- [35] S. Alimperti, H. You, T. George, S. K. Agarwal, S. T. Andreadis, *J. Cell Sci.* **2014**, *127*, 2627.
- [36] a) N. Espagnolle, F. Guilloton, F. Deschaseaux, M. Gadelorge, L. Sensebe, P. Bourin, *J. Cell. Mol. Med.* **2014**, *18*, 104; b) B. Gokcinar-Yagci, B. Celebi-Saltik, *Cell Tissue Banking* **2017**, *18*, 501.
- [37] Y. Liu, B. Deng, Y. Zhao, S. Xie, R. Nie, *Dev., Growth Differ.* **2013**, *55*, 591.
- [38] M. W. Pfaffl, *Nucleic Acids Res.* **2001**, *29*, e45.
- [39] M. W. Pfaffl, G. W. Horgan, L. Dempfle, *Nucleic Acids Res.* **2002**, *30*, e36.